Available online at www.sciencedirect.com
ScienceDirect
Biochimica et Biophysica Acta 1773 (2007) 1534–1545
Biochimica et Biophysica Acta
BBA
www.elsevier.com/locate/bbamcr

Chromatin dynamics during DSB repair

Martin Falk, Emilie Lukasova *, Barbora Gabrielova, Vladan Ondrej, Stanislav Kozubek

Institute of Biophysics, Academy of Sciences of the Czech Republic, Kralovopolska 135, 612 65 Brno, Czech Republic

Received 19 February 2007; received in revised form 4 July 2007; accepted 9 July 2007
Available online 18 July 2007

Abstract

We show that double strand breaks (DSBs) induced in chromatin of low as well as high density by exposure of human cells to γ-rays are repaired in low-density chromatin. Extensive chromatin decondensation manifested in the vicinity of DSBs by decreased intensity of chromatin labelling, increased H4K5 acetylation, and decreased H3K9 dimethylation was observed already 15 min after irradiation. Only slight movement of sporadic DSB loci for short distances was noticed in living cells associated with chromatin decondensation around DSBs. This frequently resulted in their protrusion into the low-density chromatin domains. In these regions, the clustering (contact or fusion) of DSB foci was seen *in vivo*, and *in situ* after cell fixation. The majority of these clustered foci were repaired within 240 min, but some of them persisted in the nucleus for several days after irradiation, indicating damage that is not easily repaired. We propose that the repair of DSB in clustered foci might lead to misjoining of ends and, consequently, to exchange aberrations. On the other hand, the foci that persist for several days without being repaired could lead instead to cell death.

Keywords: Chromatin structure; DNA damage; Double-strand breaks (DSB); DNA repair; Exchange aberration; Genomic instability

1. Introduction

Cells have developed sophisticated ways to deal with exposure to toxic agents in our environment. In particular, cells must be able to respond appropriately when their DNA has been damaged, either by natural processes or by exposure to chemicals or ionizing radiation. The most serious damage induced in DNA is interruption of its integrity resulting in double-strand breaks (DSBs). Improper repair of DSBs can lead to the development of cancer. Once a cancer has developed, radiation and chemotherapy are used to damage DNA so as to kill the tumour cells. Thus, recognition of how cells respond to DNA damage is critical for understanding both the development of cancer and its therapy. The first molecular events that happen in cells after DNA breakage following exposure to ionizing radiation have been identified [1,2]. Immediately after DSB induction, histone H2AX, a variant of H2A, is phosphorylated at its C-terminal serines (Ser136 and Ser139) by ATM and other phosphatidylinositol 3-kinases [1] at the site of the DSB. ATM activated by DSB formation phosphorylates a multitude of proteins that take part in a damage response pathway [3,4]. Phosphorylated H2AX (γH2AX) can be detected within minutes after the induction of DSBs, and is involved in recruitment to the sites of DSBs of other known proteins of the DNA repair signalling pathway, including NBS1/MRE11/Rad50, Brca1 and 53BP1 [5–9]. Phosphorylated H2AX does not just localize at the sites of DNA breakage, but quickly spreads to the surrounding megabase region. It is likely that this build up of γH2AX around the DSB is the signal that leads to the retention of DNA damage-response factors [5,10,11]. γH2AX may serve as a docking site for these proteins [5] or alternatively, modulate chromatin structure and thus indirectly facilitate their accumulation [12]. Chromatin structure and dynamics are strongly suspected of playing an important role in the regulation and facilitation of DNA repair [13–15]. Since genomic DNA is packed into highly organized, more or less condensed chromatin, it is conceivable that this structure must be relaxed to allow access to damaged DNA of an array of repair protein complexes [16–18]. Decondensation to allow assembly and function of huge multi-protein complexes is not unprecedented in molecular biology; it has been extensively documented, for example, at sites of gene transcription [19–21]. An

* Corresponding author. Tel.: +420 541517165; fax: +420 541240498.
E-mail address: lukasova@ibp.cz (E. Lukasova).

0167-4889/$ - see front matter © 2007 Elsevier B.V. All rights reserved.
doi:10.1016/j.bbamcr.2007.07.002

enduring question is whether chromatin also undergoes decondensation in regions of induced DSBs. Evidence suggests that such process is indeed induced by DNA damage, including DSBs [16–18]. Recently, local chromatin relaxation in the vicinity of DSBs has been demonstrated in yeast [22], and a similar process, independent of ATM, has been shown in mammalian cells [14,23]. The results of Ziv et al. [18] show that DSBs induce an ATM-dependent wave of chromatin relaxation, starting in the vicinity of DSBs and quickly extending into the entire genome as a result of the action of the ATM-phosphorylated protein KAP-1. The authors propose [18] that this global, ATM- and KAP-1-dependent chromatin relaxation that follows the local ATM-independent relaxation [14] may create the chromatin configuration that is essential for a fully efficient repair process.

Experimental evidence of chromatin decondensation induced by DSBs has been obtained by several laboratories; however, it does not provide unequivocal information about the possible regional movement of damaged DNA during this decondensation. Results of experiments dealing with this movement are contradictory [14,24–26]. The data available on DSB mobility were obtained after irradiation of cells with radiation of different quality high LET α-radiation (^{241}Am, LET > 20 keV/μm, in [24]), low energetic X-rays (synchrotron-generated ultrasoft X-rays, <5 keV in [25]) and local laser beams (e.g. argon ion UV laser, 364-nm emission line, in [14]; UV-A pulse nitrogen laser, 337 nm emission line in [26]) resulting in different local concentration of DSBs (clustered or single DSBs) [14,24–26]. Local release of high energy by high LET α-particles induces large numbers of DSBs in close proximity to each other, which could produce DNA fragmentation, unlike low LET X-rays and γ-rays that induce isolated DSBs. Bekker-Jensen et al. [8] showed that DSB yields per a nuclear volume obtained with UV-A (λ = 337 nm) laser were equivalent to about 10 Gy of ionizing radiation (delivered by X-ray generator, 150 kV; 15 mA; dose rate 2.18 Gy/min).

In this work, we contribute to the elucidation of chromatin structure and dynamics in the vicinity of DSBs induced by sparsely ionizing γ-rays of ^{60}Co (1.1 MeV, 1 Gy/min), in human fibroblasts and MCF7 mammary carcinoma cells. Our results show chromatin decondensation manifested by a decrease of intensity of chromatin labelling, increase of H4K5 acetylation and decrease of H3K9 dimethylation at sites of DSBs. A limited "movement" associated with chromatin decondensation and protrusion of DSBs into the low-density chromatin can be seen *in vivo* and *in situ* after cell fixation. Some of clustered foci persisted in the nucleus for several days after irradiation, indicating damage that was only reparable with difficulty.

2. Materials and methods

2.1. Cell culture and transfection

Human MCF7 mammary carcinoma cells and human lung fibroblasts 04-147 were grown in DMEM medium supplemented with 10% fetal calf serum (FCS) and standard antibiotics. To get transient expression of NBS1-GFP (a gift from J. Lukas), HP1β-GFP (a gift from T. Misteli), PML-GFP (a gift from M. Faretta), the cells were transfected with the GFP constructs using Lipofectamine 2000 (Invitrogene) according to the manufacturer's instructions and used for observation of protein movement 12 h after transfection, and within 30 min after irradiation. Changes in chromatin structure in regions of DSBs and breaks displacement were studied in cells co-transfected with H2B-GFP (Clontech) and pm53BP1-RFP (a gift from J. Lukas), using Fugene HD (Roche). The cells were irradiated with the dose of 1 Gy of ^{60}Co γ-rays, 35 h after transfection and immediately observed.

2.2. Cell synchronization, irradiation, fixation, permeabilization and immunostaining

Cells used for irradiation were in the G1 phase of the cell cycle (Fig. 1). Synchronization of cells in the G0 phase of the cell cycle was achieved by incubation of confluent culture of human fibroblasts without serum for 4 days. The cells were trypsinized and plated on microscope slides where they were cultured in the presence of 10% FCS. After 12 h of incubation, the cells were irradiated with γ-rays from ^{60}Co and either fixed immediately or incubated for various periods of time before fixation. The doses of γ-rays were 1.0, 1.5, 4.5 and 7 Gy (1 Gy/min).

Cells harvested at different time intervals after irradiation (5, 30, 120, or 240 min and 3 or 5 days) were washed twice for 3 min each in PBS (140 mM NaCl, 2.7 mM KCl, 1.5 mM KH_2PO_4, 6.5 mM Na_2HPO_4; pH 7.2), fixed with 4% freshly prepared paraformaldehyde in PBS for 10 min at 21 °C, rinsed quickly in PBS, then washed three times for 5 min each in PBS, permeabilized in 0.2% Triton X-100/PBS for 15 min at room temperature (RT), rinsed in PBS and washed twice for 5 min each. Before incubation with primary antibodies (overnight at 4 °C), the cells were blocked with 7% inactivated FCS + 2% bovine serum albumin/PBS for 30 min at RT. Antibodies from two different hosts (rabbit and mouse) were used on each slide to detect two different antigens in the same nuclei. Anti-H2AX phosphorylated at serine 139 (mouse) was from Upstate; anti-NBS1 phosphorylated at serine 343 (rabbit) from Cell Signaling; anti-acetyl histone H4 at lysine 12 (mouse) and Mre11 (rabbit) were from Upstate. Secondary antibodies were affinity purified donkey anti-mouse-FITC-conjugated, and affinity purified donkey anti-rabbit-Cy3-conjugated, from Jackson Laboratory (West Grove, PA). The mixture of both antibodies was applied to each slide (after their pre-incubation with 5.5% of donkey serum/PBS for 30 min at RT) and incubated for 1 h in the dark at RT. This was followed by washing (three times for 5 min each) in PBS. Cells were counterstained with 1 μM TOPRO-3 (Molecular Probes, Eugene, USA) in 2× saline sodium citrate (SSC) prepared fresh from a stock solution. After brief washing in 2× SSC, Vectashield medium (Vector Laboratories, Burlingame, CA) was used for the final mounting of samples.

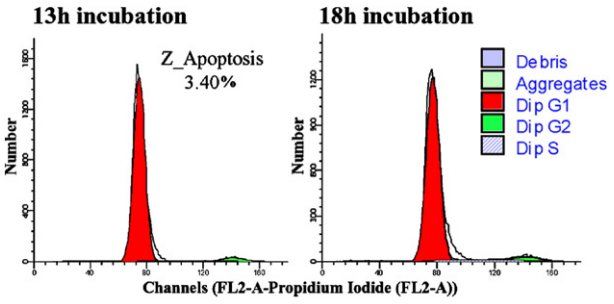

Time	G1 [%]	S [%]	G2 [%]
4h	88.81	2.61	8.59
9h	94.66	0.83	4.51
13h	95.4	0.63	3.97
18h	90.38	5.2	4.42
24h	85.43	12.96	1.6
27h	78.99	12.36	8.65

Fig. 1. Flow-cytometric monitoring of the cell cycle of human fibroblasts cultured for different periods of time (in DMEM containing 10% FCS) after their synchronization by starvation in confluence.

2.3. Cell cycle analysis

After starvation, cells were trypsinized, plated in 2×10^5 per a dish containing 5 ml of DMEM with 10% FCS and grown at 37 °C. In different time intervals, the cells were trypsinized, resuspended in the medium with 10% FCS and sedimented by centrifugation (200×*g*, 5 min, 4 °C). Cell suspension was washed in two volumes of PBS, centrifuged, resuspended in about 0.5 ml of PBS, fixed after addition of 4 ml of 70% ethanol at 4 °C for 30 min (and

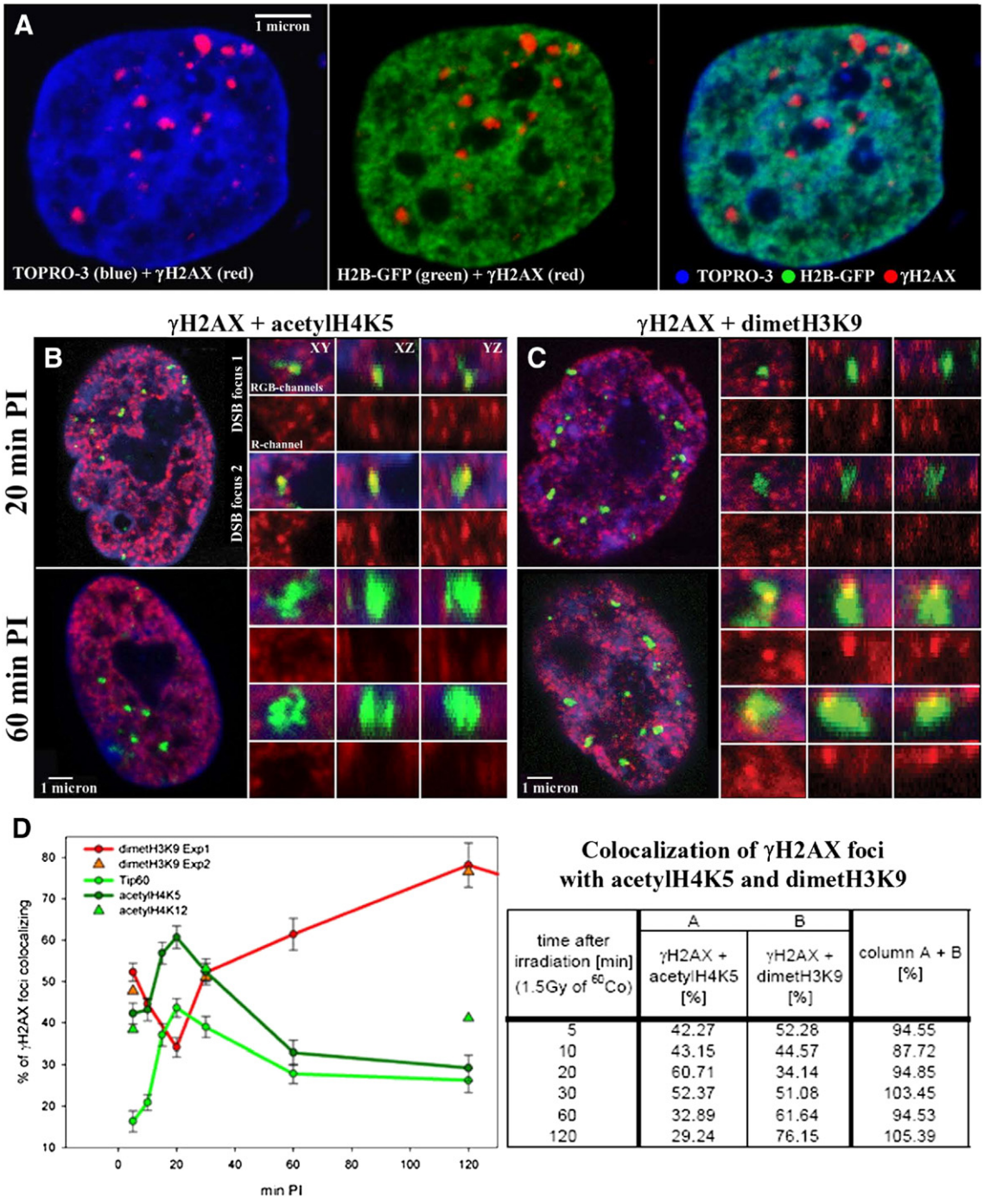

time after irradiation [min] (1.5Gy of ^{60}Co)	A: γH2AX + acetylH4K5 [%]	B: γH2AX + dimetH3K9 [%]	column A + B [%]
5	42.27	52.28	94.55
10	43.15	44.57	87.72
20	60.71	34.14	94.85
30	52.37	51.08	103.45
60	32.89	61.64	94.53
120	29.24	76.15	105.39

Fig. 2. Location of γH2AX foci relative to low- and high-density chromatin and dynamics of epigenetic modification of histones at sites of DSBs (induced with 1.5 Gy of γ-rays) during repair. (A) Cell nucleus transfected with H2B-GFP, 3D fixed 10 min PI and immunostained with anti-γH2AX (red). The nucleus was also labelled with TOPRO-3 to compare the distribution of chromatin density detected by this labelling with that of H2B-GFP. The central x–y slices through MCF7 cells are displayed to show the location of foci γH2AX relative to dense and sparse chromatin domains. (B) Central slices (0.2 μm thick) through the cell nuclei of human fibroblasts showing colocalization of γH2AX foci (green) with acetylH4K5 (red) at different times after irradiation (PI). Nuclei were fixed at 20 or 60 min PI (upper and bottom panel, respectively), immunostained with anti-γH2AX and anti-acetylH4K5 and counterstained with TOPRO-3 (blue). Right: x–y, x–z and y–z slices (0.2 μm thick) through two γH2AX foci to show their colocalization with acetylH4K5 in all three planes. Density of acetylH4K5 at sites of γH2AX foci can be seen separately in the red channel. (C) The same figure as B but for nuclei immunostained by anti-dimethylH3K9 antibody (red) in addition to γH2AX (green). Other description is the same as in B. (D) Dynamic changes of H4K5 acetylation and H3K9 dimethylation at sites of γH2AX foci during the time after cell irradiation.

maintained at this temperature until the cells of all time intervals were fixed), then centrifuged (200×*g*, 5 min, 4 °C) and washed with PBS. DNA was labelled with propidium iodide in 0.5 ml of Vindel solution (1 ml 1 M Tris, pH 8.0, +1 mg RNAsa (Sigma R-5503) +100 μl NP-40+60 mg NaCl+5 mg propidium iodide, completed to 100 ml H_2O) for 30 min at 37 °C. The cells were fractionated according to the DNA content by flow-cytometry using the FACSCalibur device (Becton Dickinson, San Jose, California, USA) with argon laser, the excitation maximum 488 nm. In each sample, 2×10^4 of cells were analysed. Fractions of cells in different phases of the cell cycle were estimated using the ModFit 3.0 software (Verity Software House, Topsham, California, USA). The results are shown for different periods of time after synchronization in Fig. 1. It can be seen that 13 h after starvation, 95.4% of cells are still in the G1 phase.

2.4. Image acquisition and microscopy

An automated Leica DM RXA fluorescence microscope (Leica, Wetzlar, Germany), equipped with an oil immersion Plan Fluotar objective (100×/NA 1.3), a CSU 10a Nipkow disc (Yokogawa, Japan) for confocal imaging, a CoolSnap HQ CCD-camera (Photometrix, Tuscon, AZ, USA) and an Ar/Kr-laser (Innova 70C Spectrum, Coherent, Santa Clara, CA, USA), were used for image acquisition [27,28]. Automated exposure, image quality control and other procedures were performed using FISH 2.0 software [27,28]. The exposure time and dynamic range of the camera in the red, green and blue channels were adjusted to the same values for all slides to obtain quantitatively comparable images. Forty serial optical sections were captured at 0.2-μm intervals (along the *z*-axis). For observation of living cells, an iXon DV 887ECS-BV (Andor) camera was used together with the 3D viewer software [29].

2.5. Living cell observation and time-lapse microscopy

Two types of *in vivo* observations were performed: short and medium-term. For short-term experiments, "2D" images consisting of a few (3–5) confocal slices with a z-step of 0.3–0.5 μm were acquired in extremely short intervals (20–500 ms) for a period of approximately 1.5 min. For medium-term observations, 40 optical sections were captured (3D images) with a 0.2–0.3 μm z-step. Intervals of 50 s were allowed between individual stacks of 40 sections, and observations were continued for a total of 20 min. The light exposure was kept as low as possible to avoid phototoxic effects. Double transfected cells with H2B-GFP and pm53BP1-RFP were observed in 5 min intervals until 30 min PI, followed by 10 min intervals until 60–120 min PI. In each interval, 15 slices with a z-step of 0.4 μm were taken. The temperature (37 °C) of medium and the 5% concentration of CO_2 in the atmosphere were kept constant during observation.

2.6. Analysis of experimental data and motion of loci

The off-line image analysis and tracking (2D, 3D) of fluorescence signals were done with the FISH 2.0 software and a 3D image viewer [27–29]. Coordinates were taken at the centre of gravity of the visualized objects, and corrected for rotation of the cell nucleus and drift of the images during longer time-lapse observations. The objects were traced in the time-lapse series on the basis of matching algorithms. In 2D, the distances between two signals were calculated using the equation: $d=\sqrt{(x_1-x_n)^2+(y_1-y_n)^2}$; or in 3D: $d=\sqrt{(x_1-x_n)^2+(y_1-y_n)^2+(z_1-z_n)^2}$, where x_1, y_1 and z_1 (x_n, y_n and z_n) were coordinates for the first measurement and the nth measurement of the same object. The mean d^2 was calculated from individual d_i^2 values of all

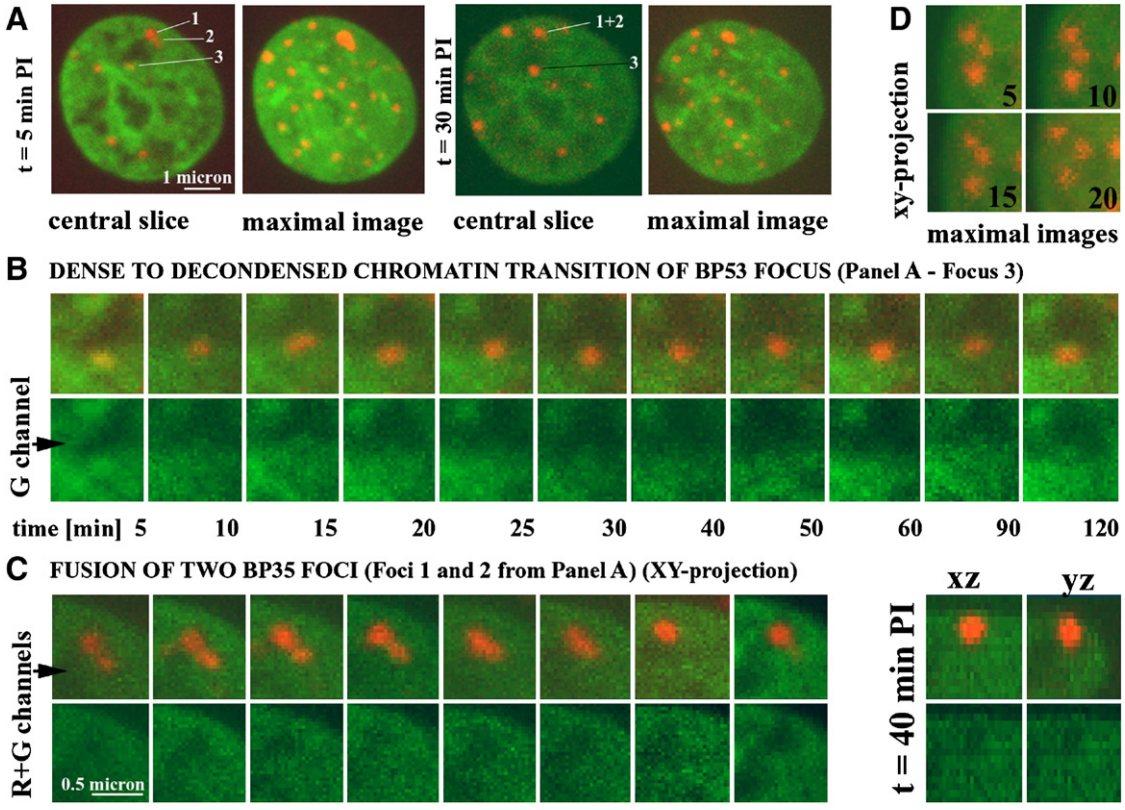

Fig. 3. Changes of chromatin density observed *in vivo* at the sites of DSBs (presented as 53BP1-RFP foci) and their displacements after γ-irradiation of MCF7 cells. (A) Central slices (0.4 μm) and maximal images in x–y plane of human MCF7 cells double-transfected with 53BP1-RFP and H2B-GFP proteins, irradiated with a dose of 1 Gy of γ-rays are displayed at 5 min (left panel) and 30 min PI (right panel). Localization of three 53BP1 foci (red) is shown relative to chromatin density (H2B-GFP, green). (B) Displacement of the focus 3 from dense (intensively green) to sparse (faintly stained) chromatin is shown in detail during the PI time (from 5 to 120 min PI). (C) Fusion of the foci 1 and 2 during the PI time (5–50 min PI) in x–y plane; for 40 min PI also the x–z and y–z slices are displayed to demonstrate the fusion in the 3D-space. The focus 2 first relocates from dense chromatin (intensively green) to H2B-GFP faintly stained domain where it fuses together with the locus 1. (D) Short-distance movement of another three 53BP1 foci (red) monitored from 5 to 20 min PI, in 5-min intervals.

Table 1
Dynamics of DSB foci (RFP-53BP1) location relative to chromatin density detected as GFP-H2B fluorescence intensity, during PI time after irradiation of MCF 7 cells with the dose of 1 Gy of γ-rays

Time PI [min]	No of foci in chromatin of different density			
	Low-density chromatin	Dense chromatin	Border of low-density and dense chromatin	Total number of foci
5	14	12	7	33
10	16	10	7	33
15	17	6	8	31
20	15	6	6	27
30	14	5	6	25
40	13	3	4	20
50	10	2	5	19
60	9	2	6	17

Dynamics of DSB foci (RFP-53BP1) location relative to low- and high-density chromatin detected as GFP-H2B fluorescence intensity, during PI time after irradiation of MCF 7 cells with the dose of 1 Gy of γ-rays.

possible signal pairs at the particular time point. The mean difference of d^2 (mean Δd^2) was calculated at each time point (t) as $\Delta d^2=(d_t-d_{t+\Delta t})^2$, where Δt was the time interval between measurements.

Evaluation of data and statistical analyses was performed using the Sigma Plot statistical package (Jandel Scientific). When required, measured distances were normalized to the nuclear radius [% of R] so as to be comparable between nuclei.

3. Results

3.1. Chromatin dynamics and epigenetic modifications in the proximity of DSBs during the post-irradiation period

DSBs induced by a dose of 1.5 Gy of ^{60}Co γ-rays were detected in fixed cells by an antibody against γH2AX as soon as 5 min post-irradiation (PI). At this time, the small γH2AX foci were dispersed throughout the nucleus with the majority of these lesions (about 70%) in weakly stained (low-density) and borderline chromatin. However, in cells fixed later after irradiation (PI=30, 120 or 240 min), the γH2AX foci were progressively extending, and protruded from the chromatin intensely labelled by TOPRO-3 or H2B-GFP (Fig. 2A) into the weakly stained chromatin "holes". This observation indicates decondensation of higher-order chromatin structure around the DSBs or DSB movement. To discriminate between changes of higher-order chromatin structure driven by chromatin decondensation or real movement of DSB foci, we analysed epigenetic modifications and nuclear dynamics of DSBs *in situ* and *in vivo*.

Chromatin decondensation in proximity of DSBs was confirmed by a sharp increase of histone H4 acetylation at lysine 5 (H4K5) and colocalization of γH2AX with Tip60 histone acetylase (HAT) between 10 and 30 min after irradiation, with the maximum at 20 min PI (about 60% of γH2AX colocalized with acetylH4K5 at this time, Fig. 2B, D,

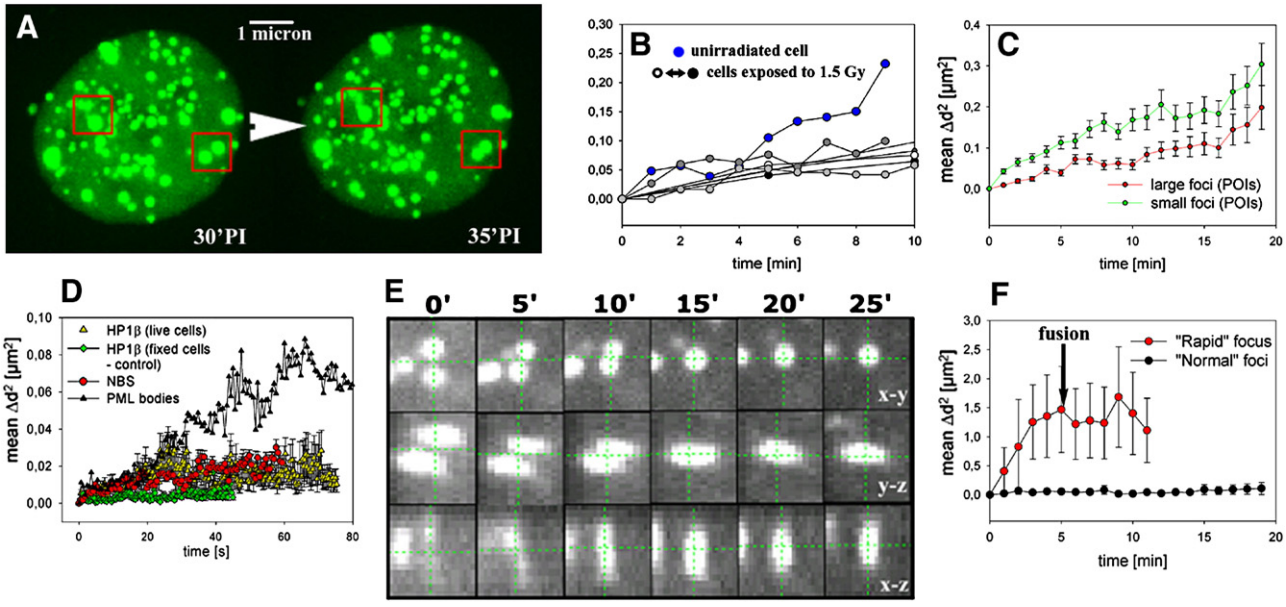

Fig. 4. Nuclear movement and fusions of DSB foci measured *in vivo* in human MCF-7 cells irradiated with 3 Gy of γ-rays. (A) Larger NBS1-GFP foci (green) framed in red, marking sites of DSBs, were tracked from 30 min (left nucleus) to 35 min (right nucleus) after exposure of cells to γ-rays. (B) The mean squared displacement (mean Δd^2) of NBS1-GFP focus before irradiation (blue) and the decreased mobility of foci after irradiation (0.03 μm²/min vs. 0.01 μm²/min) measured 10 min PI in several samples (grey). (C) Comparison of the mean squared displacement (mean Δd^2) of large (red) and small (green) NBS1-GFP foci in living irradiated cells. (D) Mean squared displacement (mean Δd^2) of NBS1-GFP foci (red) in γ-irradiated living cells measured for 60 s with a 0.5-s interval, 30 min PI. Mean Δd^2 values are also shown for HP1β in non-irradiated 3D-fixed cells (green diamonds), and in living cells (yellow triangles), representing background movement and mobility of heterochromatin, respectively, and for PML bodies (black triangles) showing the movement of a non-chromatin protein complex. (E) An example of cluster formation from spatially distinct NBS1-GFP foci (DSBs) monitored in 4D during a 25-min interval, starting 20 min PI. The cluster was formed after 15 min of monitoring and remained stable for at least next 10 min. (F) Comparison of the mean squared displacement (mean Δd^2) for normally visible (black circles) and highly mobile (red circles) NBS1-GFP foci in γ-irradiated living cells. The arrow indicates fusion of the tracked highly mobile focus with another one, and the consequent decrease of the mobility of the cluster.

and 40% colocalized with Tip60, Fig. 2D). A high level of histone H4 acetylation at lysine 12 (acetylH4K12) was also detected (about 55% of γH2AX presented the signal of acetylH4K12 at 30 min after irradiation, Fig. 2D). The sharp increase of acetylH4K5 and Tip60 localization at sites of DSBs was followed by a decrease of these signals after reaching the maximum at 20 min PI. Signals of acetylH4K5 and acetylH4K12 did not usually cover whole foci of γH2AX, but colocalized only with the edge of them, as if forming a link between the focus and denser chromatin, stained by TOPRO-3 (Fig. 2B). On the other hand, Tip60 was localized rather in the centre of H2AX foci (not shown). The rapid increase of histone

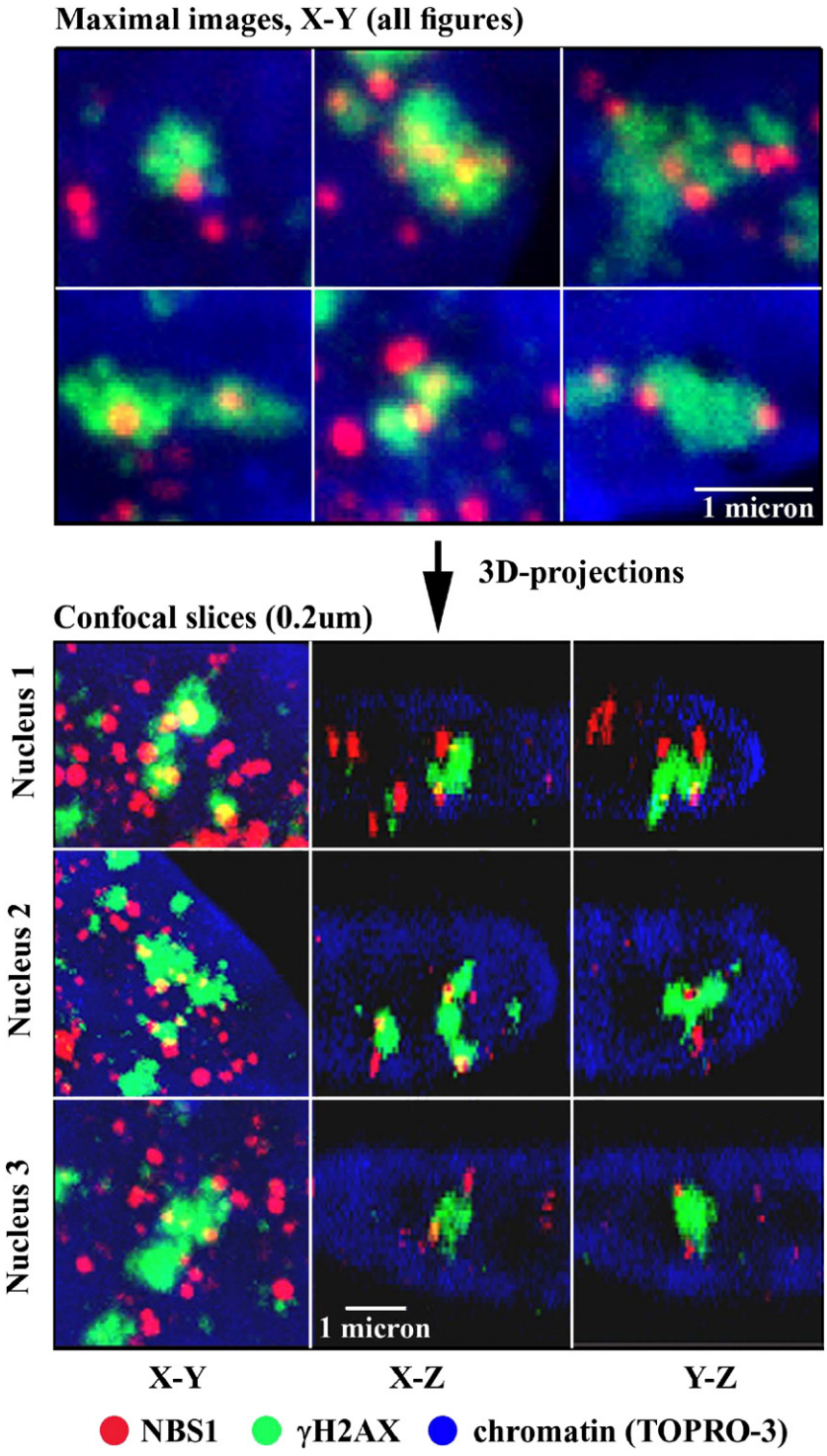

Fig. 5. γH2AX foci clustering in spatially fixed human fibroblasts irradiated with 3 Gy of γ-rays. Top: maximal images (x–y plane, 40 slices) showing clustering of γH2AX foci (green) observed between 30 min and 2 h PI; NBS1 (red), chromatin stained with TOPRO-3 (blue). Bottom: verification of clustering of γH2AX foci in 3D space: optical slices (0.2 μm) through three γH2AX clusters in x–y, y–z and x–z planes.

H4K5 acetylation was accompanied by a corresponding decrease of dimethylH3K9 in γH2AX foci (Fig. 2B–D), and inversely, the decrease of acetylH4K5 was followed by an increase of dimethylH3K9, later PI (Fig. 2B–D). Observed changes in epigenetic modifications of histones H4 and H3 seemed to complement each other and took place in a relatively short interval of time after DSB induction. The number of γH2AX foci containing a signal of dimethylH3K9 progressively increased up to about 76% at 120 min PI, when the number of foci with acetylated H4K5 was about 29% (Fig. 2D). Interestingly, while the increase of histone H4K5 acetylation accompanied by the decrease of histone H3K9 dimethylation were followed by a visible chromatin decondensation, manifested by spreading of chromatin regions with low intensity of H2B-GFP at sites of DSBs (Fig. 3A, B), the decrease of H4K5 acetylation and increase of H3K9 methylation were not followed by detectable changes of chromatin density (Figs. 2D, 3A, B).

3.2. Displacement and fusion of DSBs in living cells

To track the displacement of DSB foci, we observed living cells double-transfected with H2B-GFP and 53BP1-RFP at 5 min intervals during the PI time. Fig. 3 show that signals of 53BP1-RFP (foci 3 and 2 in 3B and 3C respectively), first located in dense chromatin (represented by an intense fluorescence of H2B-GFP), gradually protrudes into chromatin of low density (in about 15–25 min PI), where it persists to 90 min PI. This displacement was accompanied by slight changes of chromatin structure in the proximity of the signal (Fig. 3B, C; bottom rows). Relocation of all 53BP1-RFP foci relative to chromatin density, followed in 2 nuclei at 5-min intervals from 5 to 60 min PI, is evaluated in Table 1. At five minutes PI, there were about 14 and 12 foci in decondensed and dense chromatin, respectively, and 7 in the boundary area of both chromatin domains. The number of foci in decondensed chromatin increased to 16 at the expense of condensed one in 10 min PI. The most marked changes in foci location were observed at 15 min PI, when the number of foci in condensed chromatin decreased to 6; on the other hand, it increased in decondensed and "borderline" chromatin domains. In 60 min PI, the number of foci in condensed chromatin decreased to 2; however, it decreased also in decondensed and borderline chromatin, probably as the result of DSB repair. According to visual inspection, the changes of higher-order chromatin structure observed at DSB sites consisted in protrusion of 53BP1 foci into decondensed chromatin domains rather than in their real longer-distance displacement. In general, the movement of foci was rare; nevertheless, we identified also some foci with a higher mobility. The slight movement of three 53BP1-RFP foci during 15 min (5–20 min PI) can be seen in Fig. 3D.

In order to quantify the DSB mobility exactly and confirm these observations also for other repair proteins, we tracked computationally foci of GFP-tagged NBS1 protein in both transiently transfected control and γ-irradiated MCF7 cells (dose of 3 Gy); larger NBS1 foci appeared only in irradiated cells (Fig. 4A). The mean squared displacement (mean Δd^2) of NBS1-GFP also revealed a decrease in mobility of NBS1-GFP foci after irradiation (0.03 μm^2/min vs. 0.01 μm^2/min) measured 10 and 20 min PI respectively (Fig. 4B), with a greater effect for larger NBS1 foci (0.02 μm^2/min vs. 0.008 μm^2/min) (Fig. 4C). This indicates that larger NBS1 foci become attached to DSB sites and can be therefore used to determine their mobility. Short-term measurements of the movement of NBS1 foci were performed with a very short period of 20–500 ms to eliminate "shivering" of the whole nucleus. The mean Δd^2 calculated from changes of distances between all possible pairs of large NBS1 foci revealed similar mobility of NBS1 (0.025 μm^2/min) and HP1β protein (0.020 μm^2/min), characteristic of proteins bound to "immobile" heterochromatin (Fig. 4D). This value was significantly higher than the total background movement determined with NBS1 in spatially fixed cells (0.005 μm^2/min), but lower than that of PML bodies (0.070 μm^2/min) in living cells, which represent an example of a non-chromatin-bound and therefore more mobile nuclear protein complexes (Fig. 4D). However, tracking of individual NBS1 signals instead of measurement of mean Δd^2 revealed noticeable movement of a small proportion of foci (Fig. 4A, E). The mobility of such a highly-mobile NBS1 focus is quantified in Fig. 4F (about 0.37 μm^2/min in the initial phase of movement).

In some (relatively rare) cases, two or more NBS1 foci (DSBs) fused together and formed larger, more stable clusters, later dissociating into individual foci or persisting in nuclei (Fig. 4A, E interval, 2.5–12 min). To exclude that this observation reflects a tendency of over-expressed protein to form GFP-aggregates, the experiment was performed also with cells expressing very low levels of 53BP1-RFP protein. The number of foci in double transfected (53BP1-RFP+H2B-GFP) living cells corresponded to the number of γH2AX foci immuno-detected in fixed cells irradiated with the same dose (1 Gy) of γ-rays; it indicates that 53BP1-RFP is not highly expressed and that its foci really represent DSBs. Similarly, as in living cells where DSBs were represented by NBS-GFP foci, a rare clustering was also observed among foci of 53BP1-RFP. A fusion of two 53BP1-RFP foci located close to each other is shown in Fig. 3A, C. One of these foci (focus 1, Fig. 3A, C) was located in decondensed and one (focus 2, Fig. 3A, C) in condensed chromatin at the beginning of the observation (5 min PI); during the continuing PI time, the latter one displaced progressively to the other (located in decondensed chromatin) until their fusion at 25–40 min PI.

Consequently, large populations of fixed cells were studied to quantify clustering of DSB foci. Also in the fixed cells, accumulation of γH2AX+NBS1 foci in the restricted space of the chromatin "holes" was observed that occasionally resulted in clustering of two or more foci (Fig. 5). The number of these clusters increased with the PI time (3 clusters was the mean per nucleus 120 min PI) when an increasing percentage of γH2AX foci localized in decondensed chromatin.

To monitor DSB movement and clustering relative to the ongoing repair process, we analysed the dependence on PI time of the interaction of NBS1 and Mre11 proteins (both members of the MRN complex) with DSBs (γH2AX signals), and of the nuclear localization of DSBs in functionally different chromatin domains (condensed and decondensed chromatin) (Fig. 6A, B). In nuclei

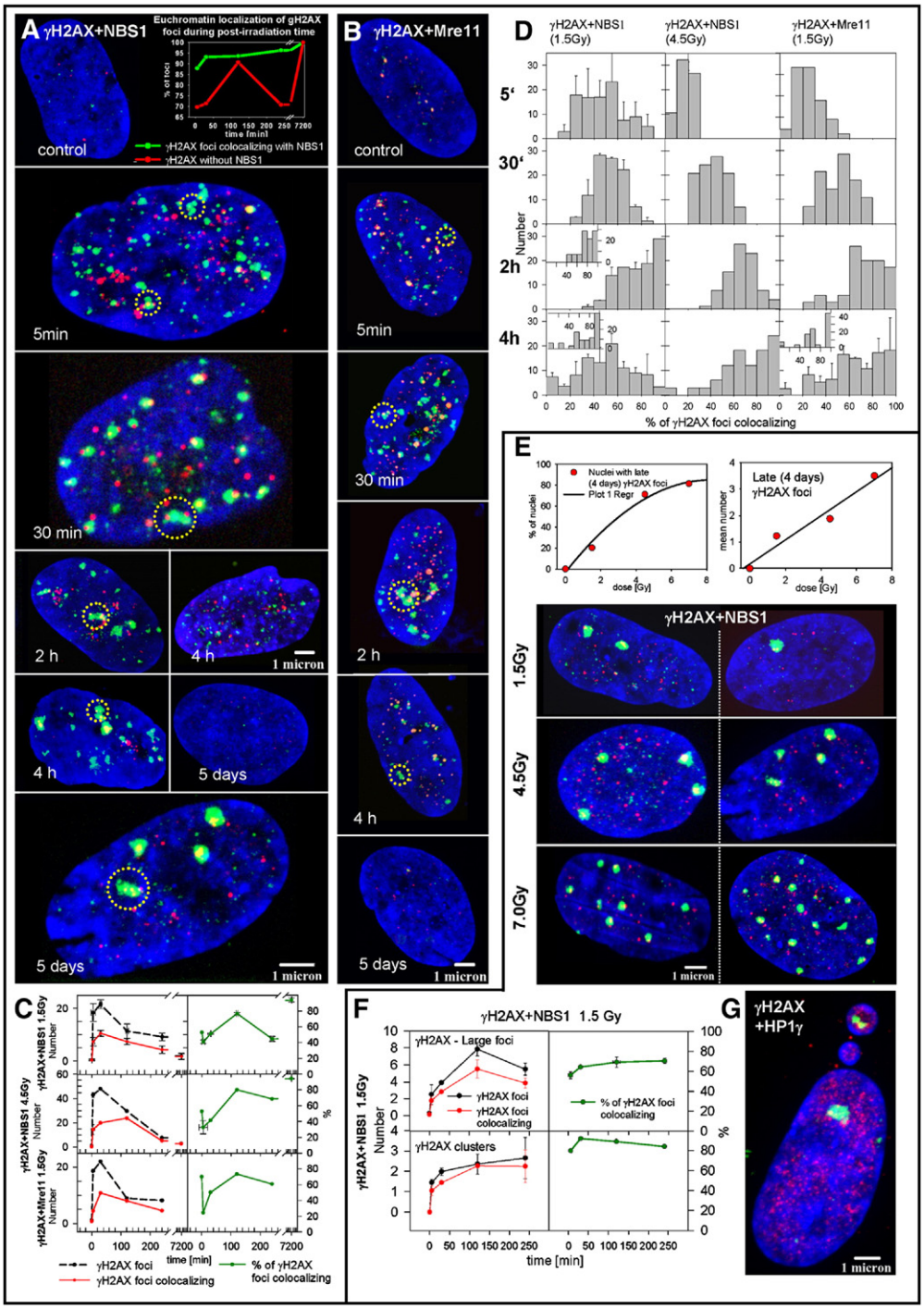

Fig. 6. The development of γH2AX foci, their colocalization with NBS1 and Mre11, and their dependence on time after irradiation. γH2AX foci (green) and their colocalization with MRN-complex components (A) NBS1 (red), and (B) Mre11 (red) during a long PI period (5 min to 5 days). The inset graph in (A) compares the dependence on PI time of the location in sparse chromatin (weak TOPRO-3 staining) of γH2AX foci that do not (red line) or do (green line) colocalize with NBS1 Yellow circles mark clustered γH2AX foci. (C) Time-dependent colocalization of γH2AX foci (clouds) with NBS1 and Mre11 from 5 min to 5 days PI in human fibroblasts irradiated with 1.5 or 4.5 Gy of γ-rays. Left: number of γH2AX foci (black circles, dashed line) observed at a particular PI time, and the number of γH2AX foci colocalizing with NBS1 or Mre11 protein (red circles, continuous line). Right: percentage of γH2AX clusters. Vertical and horizontal error bars represent SD and SE respectively. (D) Distributions of nuclei according to the percentage of γH2AX foci colocalizing with NBS1 or Mre11 proteins at different PI times. Inserted graphs show the same distributions when only large γH2AX foci were scored. (E) Left: percentage of irradiated human fibroblasts containing γH2AX foci 4 days PI plotted against the absorbed γ-ray dose [Gy]. Right: linear relation between the mean number of γH2AX foci persisting in nuclei 4 days PI, and the absorbed dose [Gy] (only nuclei containing γH2AX foci were scored). Maximal images of nuclei containing γH2AX foci (green) 4 days PI for doses of 1.5, 4.5 and 7.0 Gy. The increase in the number of γH2AX foci per nucleus with the absorbed dose, and an almost complete colocalization of γH2AX foci (green) with NBS1 (red), are clearly visible. (F) Lower repair efficiency of large, and especially clustered, γH2AX foci (clouds) compared with the "usual" DSB population (see Fig. 4C for comparison) is demonstrated by their long persistence G: Maximal image of the nucleus of a human fibroblast accompanied by micronuclei, one containing a double-minute (green). The cells were irradiated with 4.5 Gy of γ-rays and fixed 4 days PI.

fixed by paraformaldehyde, γH2AX foci detected 5 min after irradiation did not yet colocalize with NBS1 in all cases; at that time, on average only 41% and 24% of γH2AX foci visually colocalized with NBS1 and Mre11 respectively, even if there were enough of free foci of these proteins, especially at short PI time. (These foci could represent, likely, free proteins not yet coupled with the MRN complexes or the MRN complexes not bound to DSBs; but, in some cases, small dots might represent a background signal). During the PI period, the size and frequency of colocalizing γH2AX foci increased up to 2 h (76% for NBS1 and 73% for Mre11) and the number of free NBS1 and Mre11 foci decreased (Fig. 6A–C). Four hours PI, colocalization of both proteins with γH2AX foci decreased to 44–60% (Fig. 6C) as the proportion of nuclei with repaired DSBs increased (decaying γH2AX foci have low colocalization with NBS1, Fig. 6A); large γH2AX foci, however, still persisted in a subgroup of nuclei, colocalizing with NBS1 and Mre11 (Fig. 6A, D–G).

The percentage of γH2AX foci located in low-density chromatin increased from a few minutes up to 2 h PI, and decreased again at 4 h (Fig. 6A, inset graph), corresponding to the curve of γH2AX colocalization with the MRN-complex (Fig. 6C). The frequency of DSBs associated with large repair complexes (γH2AX+NBS1 foci) was very high (about 90%) at all PI times in low-density chromatin, with a slight tendency to increase gradually (Fig. 6A, inset graph).

Thus, from 30 min to about 2 h PI, almost all foci colocalized with NBS1 and Mre11 proteins, indicating that the repair process is going on (Fig. 6A, B) (NBS1 represents here the MRN complex, which also contains Mre11 and Rad50). These actively repaired DSBs prevailing in the nucleus were almost all located in low-density chromatin, unlike the breaks detected early (2–5 min) after irradiation (Figs. 2A, 3, 6A). Moreover, increasing localization of γH2AX foci in low-density chromatin was associated with a higher probability of clustering; clustered DSB lesions started to appear within minutes after irradiation (Fig. 6A, B yellow circles) and their number increased slightly with PI time (data not shown). Clustering appeared between DSBs protruding into the same chromatin "hole" (lesions A and B at Fig. 7), even when another lesion (lesion C at Fig. 7) closer to one of the clustered breaks was present but separated by condensed chromatin and protruding into another chromatin "hole".

3.3. DSBs persisting for several days after irradiation

Very large and intense γH2AX foci persisted in a fraction of nuclei even 5 days PI; the fraction of nuclei containing such foci was quadratically dependent on the dose absorbed (from 18% with 1.5 Gy to >80% with 7 Gy) (Fig. 6E, left graph). The average number of late foci per nucleus depended linearly on the absorbed γ-ray dose (from 1 with 1.5 Gy to 3.5 with 7 Gy) (Fig. 6E, right graph) and almost all of them colocalized with NBS1 (Fig. 6A, C, nuclei at Fig. 6E). Some of the late foci were clearly clustered lesions, persisting for a long time without being repaired (colocalizing with the MRN-complex). Lower repair efficiency of large and especially clustered γH2AX foci was shown by a significantly slower decrease in their number with PI time (long time persistence) compared with the rest of the DSB population (Fig. 6F). Sometimes, a micronucleus, sporadically having a γH2AX focus, was observed adjacent to a cell still containing unrepaired foci. It is not clear, however, when these micronuclei arise; whether it is before or after the cell irradiation, and whether or not cell division is required for their formation (Fig. 6G).

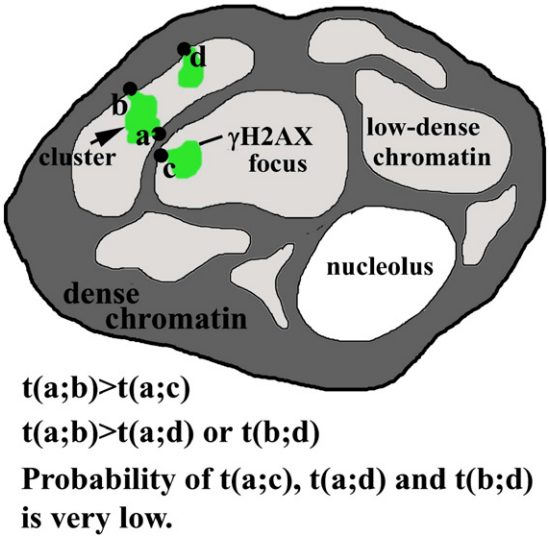

Fig. 7. Schematic drawing of a cell nucleus showing the protrusion of γH2AX (DSB) (green) from the dense chromatin into the low-density chromatin "holes". Accumulation of more DSBs in the same hole results sometimes in their clustering (a and b), especially after higher radiation doses. *t*(*a*;*b*) indicates probability of a translocation (*t*) between fragments of chromosomes corresponding to loci (breaks) *a* and *b*. Sometimes DSBs induced in close proximity (a and c) protrude into different chromatin "holes", which probably lowers the chance of chromatin exchange between them.

4. Discussion

In this work we bring new insights into the crucial question of the mobility of DSBs induced by irradiation of cells with γ-rays. Evidence of DSB mobility is extremely important, especially in connection with recognition of the possible mechanism of formation of exchange aberrations. Despite intensive research, we still do not know enough about the topology of DSBs and chromatin structure at the site of this DNA damage.

It is obvious that all nuclear processes that use DNA as a template require accessibility for specific protein machineries, which could be gained by chromatin relaxation. It is well known that histone acetylases (HAT) are important chromatin modifiers that play a central role in chromatin relaxation [30]. Recent results showed that binding of HAT Tip60 to the chromatin surrounding sites of DSBs was accompanied by chromatin acetylation [23] allowing accumulation of repair proteins and DSB repair by homologous recombination. These processes were prevented if HAT function was inhibited, indicating the necessity of chromatin acetylation for DSB repair. We show that the frequency of HAT colocalization with γH2AX foci increases rapidly immediately after irradiation and decreases after reaching the maximum at 20 min PI (Fig.

2). The increase and decrease of the enzyme colocalization was accompanied by corresponding changes of H4K5 acetylation at γH2AX foci. It can be seen that neither acetylH4K5 nor acetylH4K12 cover the whole foci of phosphorylated H2AX but colocalize only with their parts. We can only speculate about the reason for this phenomenon. Phosphorylation of H2AX in the DSB region may be sufficient to relax chromatin in the close vicinity of a break and that acetylation is needed to open the more distant chromatin. It is also possible that phosphorylation of H2AX hampers acetylation in this region. The increased acetylation of H4K5 in regions of DSB foci was accompanied by the decreased dimethylation of H3K9. These epigenetic modifications of H4 and H3 histones, characteristic for decondensed chromatin, were soon (40 min PI) replaced by histone modifications typical of condensed chromatin (decreased acetylation of H4K5 and increased methylation of H3K9 [31–33]). Relatively rapid changes of epigenetic modifications of both histones in the proximity of DSBs indicate a necessity of chromatin conversion to less condensed state during the repair. The increased H4K5 acetylation accompanied by decreased H3K9 methylation was reflected in decrease of fluorescence intensity of H2B-GFP and TOPRO-3 in regions of DSBs; however, opposite epigenetic modifications characteristic for condensed chromatin were not associated with a visible chromatin re-condensation (Fig. 2B, C, 3A, B). Instead, low intensity of chromatin labelling at sites of γH2AX foci progressively extended with the time after irradiation, up to 60 min PI in living as well as in fixed cells. These observations are difficult to explain for the time being. It is possible, that increased methylation of H3K9 in γH2AX foci could lead only to local chromatin condensation, preventing access of transcription complexes to these regions until termination of DSB repair; alternatively, it could present a signal for later chromatin condensation, after dissociation of repair proteins and/or γH2AX dephosphorylation.

We were able to visualize changes in chromatin compaction around DSBs by the decrease of H2B-GFP and TOPRO-3 fluorescence intensity within the time after irradiation, and show that chromatin structure in the vicinity of DSBs changes very soon after their induction. While at 5 min PI, DSBs were located in both condensed and decondensed chromatin (Table 1, Fig. 2A), 25 min later the majority of DSBs were observed in low-density chromatin, but usually in contact with dense chromatin at one side (Figs. 2B, C and 3B, C). This arrangement gave an impression of DSBs protruding into the chromatin "hole". The space around the DSBs appeared as a hole because of the very faint chromatin staining by H2B-GFP and TOPRO-3 in the region. Use of TOPRO-3 to determine chromatin density provides even more stringent conditions for distinguishing chromatin density than DAPI, since TOPRO-3 stains DNA, and to a lesser extent RNA. Equivalent results to those with TOPRO-3 were obtained when H2B-GFP was used to visualize chromatin (Figs. 2A, 3A, B), indicating that TOPRO-3 could legitimately be used to estimate chromatin density. Decondensation of chromatin in the proximity of DSBs induced with a dose of 10 Gy of γ-rays or with 364-nm UV laser in the presence of Hoechst 33342 (the dose equivalent to about 2.5 Gy of γ-rays) in mouse embryonic stem cells was also observed using a different approach by Kruhlak et al. [14].

What causes changes in chromatin density in the vicinity of DSBs 15 min after irradiation and later? Does it reflect the simple chromatin decondensation or active movement of DSBs from dense to less condensed areas? We tried to get the answer to this question by observing double-transfected living cells (H2B-GFP and 53BP1-RFP) in 5 min intervals during the PI time, starting 5 min PI. It follows from this observation (Fig. 3B) that the density of H2B-GFP progressively decreases in regions of 53BP1-RFP foci (DSBs), and the space of faintly labelled chromatin extends. We followed the density of chromatin labelling at sites of all 53BP1-RFP foci in two living nuclei (Table 1) and found a progressive chromatin decondensation in the vicinity of those originally located in dense chromatin; only 2 from 12 foci remained in condensed chromatin 60 min PI. In the majority of cases, foci of 53BP1-RFP (in living cells) as well as γH2AX (in fixed cells) located in the low-density chromatin were in touch with intensely labelled (condensed) chromatin (Figs. 2B, 3B) and not isolated in faintly labelled chromatin "holes". Thus, it rather indicates local chromatin decondensation than DSB movement to specific nuclear domains. The majority of foci stayed at sites of their origin and does not noticeably move. Only in rare cases, the slight movement was observed that occasionally resulted in clustering of 53BP1-RFP and NBS1-GFP foci occurring in mutual proximity (Figs. 3A, 4A). In the case of NBS1-GFP, we could not exclude that "mobile" NBS1 foci (>2%) might represent NBS1 protein already detached from chromatin instead of highly mobile DSB ends. These results show that there is no significant movement of DSBs in the irradiated cell nucleus, and that their repair proceeds at the sites of their origin, after chromatin decondensation. Our observations indicate that there is a low probability of DSB repair in condensed chromatin, in accordance with results of Ziv et al. [18] that show global chromatin decondensation starting in DSBs early after their induction.

Sometimes, several γH2AX foci appeared in the same "hole" of decondensed chromatin. Two or more of these foci were often in contact, and formed clusters 15 min and later after irradiation. This clustering may develop during decondensation of a chromatin region with two or more DSBs in mutual proximity; alternatively, it might arise from the coalescence of two proximal γH2AX foci during their movement, as it was rarely observed in living cells (Figs. 3A, E, 4). Clusters of γH2AX loci are rare early (5 min) after DSB induction, comprising about 5% of all foci (in average 1 cluster per 20 foci); nevertheless, they can be a risk factor for chromatin exchange during repair. Later after irradiation, the number of clusters increases significantly (in average 2.5 clusters per 8 foci, about 31% in 2 h PI) indicating that DSB clusters are difficult to repair.

The frequency of clusters increased with the absorbed dose, correlating with a higher number and density of DSBs, which in turn leads to an increasing probability of association of adjacent DSBs. An appearance of clustering might also result from non-functional overlapping of γH2AX foci as they enlarge during the PI period. However, some DSBs were already clustered several minutes PI, when γH2AX foci were still very small. Moreover, unlike the temporary clusters described by Kruhlak

et al. [14], at least some of the clusters we observed in living cells were stable and obviously not easily reparable, since they persisted in nuclei for hours or even days PI.

Contradictory results concerning mobility of DSBs (suggesting highly mobile and completely immobile DSBs, respectively) have been published [14,24,25]. There are most probably two reasons for this: (1) observation of changes at different PI times and phases of the cell cycle; (2) use of different kinds of radiation to induce DSBs. Petrini and Stracker [34] postulated that the late DSB foci (observed hours PI) analysed in most studies represent sites of unsuccessful repair rather than normally repaired breaks. Further, high-LET particles [24] and also microlasers [14], frequently used for DSB generation, produce a high density of DNA breaks at the site of energy deposition [35]. Such a high density of breaks (clustered breaks) may lead to chromatin fragmentation, resulting in repair difficulties. Moreover, short DNA fragments may be released, which are more mobile than the chromatin at the site of DSBs. Indeed, high mobility of DSBs and their clustering was described after exposure of cells to α-particles [24]. On the other hand, irradiation with ultra-soft X-rays resulted in immobile lesions [25]. We used γ-radiation to generate isolated DSB-breaks and monitored changes in higher-order chromatin structure from minutes up to several days PI.

As stated above, some γH2AX foci, especially clustered ones but also single foci remained in low-density chromatin even several (3–5) days after irradiation, indicating that these lesions were difficult to repair. It is not clear whether all long-lasting γH2AX foci represent not yet repaired DSBs. We observed a decrease of the number of 53BP1 foci (another marker of DSBs) to about 78% in 30 min PI and 51% in 1 h PI in living cells. In fixed cells, the number of γH2AX foci reached the maximum at 30 min PI, and then decreased to about 50% in 2 h PI. These observations are in agreement with findings of the Tomilin group [36], showing that dephosphorylation of γH2AX foci does not follow immediately after DSB rejoining, and that γH2AX persists at the sites of already repaired break for some time. How γH2AX is removed from chromatin remains unknown.

Late DSBs that persist in nuclei for 24 h and longer do not seem to be only resolved γH2AX foci, inefficiently dephosphorylated after finished repair, but rather not yet repaired lesions. Our opinion is based on the observation that two kinds of persisting γH2AX foci could be distinguished from about 4 h after irradiation. The first type is represented by fuzzy γH2AX foci, with frequency and colocalization with repair proteins progressively decreasing during PI time. These foci are supposed to be already resolved breaks. On the other hand, the foci dominating in nuclei long time PI, are intensively labelled, gradually growing, and almost all of them still colocalize with repair proteins. The evidence for a long-time persistence of DSBs in human cells exposed to very low doses of X-rays presented also Rothkamm and Löbrich [37].

The fraction of cells with the late foci and the average number of foci per nucleus, increased significantly with the absorbed dose of γ-radiation. It is possible that in some cases, cells might divide despite containing late DSBs, and DSBs appeared in parental cells as well as in their progeny. This presupposition is based on the observation that some cells were accompanied by micronuclei, some of which also contained DSBs; some authors suppose that micronuclei appear during cell division [38,39]. Division of cells containing broken DNA cannot be frequent, since it is prevented by the S-phase checkpoint that stops replication. However, there is the evidence that some specialized polymerases can sometimes bypass the broken DNA, and continue DNA replication without completing DSB repair [40]. Nevertheless, the cell cannot tolerate broken DNA for a long time, and is usually forced into apoptosis (our preliminary results).

Acknowledgments

We thank Mario Faretta (The European Institute of Oncology, Milan), Jiri Lukas (The Danish Cancer Research Centre, Copenhagen) and Tom Misteli (NIH, Bethesda, Maryland) for their gifts of plasmids and to Karel Soucek (The Institute of Biophysics ASCR, Brno) for flow-cytometric analysis.

The work was supported by the Grant Agency of the Czech Republic No. 204/06/P349 and IQS500040508, the Grant Agency of the Academy of Sciences of the Czech Republic No. IAA1065203 and the Ministry of Education of the Czech Republic No. ME 1P05OC084.

References

[1] E.P. Rogakou, D.R. Pilch, A.H. Orr, V.S. Ivanova, W.M. Bonner, DNA double strand breaks induce histone H2AX phosphorylation on serine 139, J. Biol. Chem. 273 (1998) 5858–5868.
[2] C.J. Bakkenist, M.B. Kastan, DNA damage activates ATM through intermolecular autophosphorylation and dimmer association, Nature 421 (2003) 499–506.
[3] Y. Shiloh, The ATM-mediated DNA-damage response: taking shape, Trends Biochem. Sci. 31 (2006) 402–410.
[4] C.J. Bakkenist, M.B. Kastan, Initiating cellular stress responses, Cell 118 (2004) 9–17.
[5] A. Celeste, O. Fernandez-Capetillo, M.J. Kruhlak, D.R. Pilch, D.W. Staudt, A. Lee, R.F. Bonner, W.M. Bonner, A. Nussenzweig, Histone H2AX phosphorylation is dispensable for the initial recognition of DNA breaks, Nat. Cell Biol. 5 (2003) 675–679.
[6] C. Lukas, J. Falck, J. Bartkova, J. Bartek, J. Lukas, Distinct spatiotemporal dynamics of mammalian checkpoint regulators induced by DNA damage, Nat. Cell Biol. 5 (2003) 255–260.
[7] O.A. Sedelnikova, D.R. Pilch, C. Redon, W.M. Bonner, Histone H2AX in DNA damage and repair, Cancer Biol. Ther. 2 (2003) 233–235.
[8] S. Bekker-Jensen, C. Lukas, R. Kitagawa, F. Melander, M.B. Kastan, J. Bartek, J. Lukas, Spatial organization of mammalian genome surveillance machinery in response to DNA strand breaks, J. Cell Biol. 173 (2006) 195–206.
[9] I.M. Ward, K. Minn, K.G. Jorda, J. Chen, Accumulation of checkpoint protein 53BP1 at DNA breaks involves its binding to phosphorylated histone H2AX, J. Biol. Chem. 278 (2003) 19579–19582.
[10] C.H. Bassing, W. Swat, F.W. Alt, The mechanism and regulation of chromosomal V(D)J recombination, Cell 109 (2002) S45–S55.
[11] A. Celeste, S. Petersen, P.J. Romanienko, O. Fernandez-Capetillo, H.T. Chen, O.A. Sedelnikova, B. Reina-San-Martin, V. Coppola, E. Meffre, M.J. Difilippantonio, C. Redon, D.R. Pilch, A. Olaru, et al., Genomic instability in mice lacking histone H2AX, Science 296 (2002) 922–927.
[12] O. Fernandez-Capetillo, S.K. Mahadevaiah, A. Celeste, P.J. Romanienko, R.D. Camerini-Otero, W.M. Bonner, K. Manova, P. Burgoyne, A. Nussenzweig,

H2AX is required for chromatin remodelling and inactivation of sex chromosomes in male mouse meiosis, Dev. Cell 4 (2003) 497–508.
[13] C. Lukas, J. Bartek, J. Lukas, Imaging of protein movement induced by chromosomal breakage: tiny 'local' lesions pose great 'global' challenges, Chromosoma 114 (2005) 146–154.
[14] M.J. Kruhlak, A. Celeste, G. Dellaire, O. Fernandez-Capetillo, W.G. Muller, J.G. McNally, D.P. Bazett-Jones, A. Nussenzweig, Changes in chromatin structure and mobility in living cells at sites of DNA double-strand breaks, J. Cell Biol. 172 (2006) 823–834.
[15] J.I. Loizou, R. Murr, M.G. Finkbeiner, C. Sawan, Z.Q. Wang, Z. Herceg, Epigenetic information in chromatin: the code of entry for DNA repair, Cell Cycle 5 (2006) 696–701.
[16] A.M. Gontijo, C.M. Green, G. Almouzni, Repairing DNA damage in chromatin, Biochemie 85 (2003) 1134–1147.
[17] A. Verger, M. Crossley, Chromatin modifiers in transcription and DNA repair, Cell. Mol. Life Sci. 61 (2004) 2154–2162.
[18] Y. Ziv, D. Bielopolski, Y. Galanty, C. Lukas, Y. Taya, D.C. Schultz, J. Lukas, S. Bekker-Jensen, J. Bartek, Y. Shiloh, Chromatin relaxation in response to DNA double-strand breaks is modulated by a novel ATM- and KAP-1 dependent pathway, Nat. Cell Biol. 8 (2006) 870–876.
[19] W.G. Muller, D. Walker, G.L. Hager, J.G. McNally, Large-scale chromatin decondensation resulted by transcription from a natural promoter, J. Cell Biol. 154 (2001) 33–48.
[20] A.C. Nye, R.R. Rajendran, D.L. Stenoien, M.A. Mancini, B.S. Katzenellenbogen, A.S. Belmont, Alteration of large-scale chromatin structure by estrogen receptor, Mol. Cell Biol. 22 (2002) 3437–3449.
[21] A.E. Carpenter, S. Memedula, M.J. Plutz, A.S. Belmont, Common effect of acidic activators on large-scale chromatin structure and transcription, Mol. Cell Biol. 25 (2005) 958–968.
[22] T. Tsukuda, A.B. Fleming, J.A. Nickoloff, M.A. Osley, Chromatin remodelling of a DNA double-strand break site in *Saccharomyces cerevisiae*, Nature 438 (2005) 379–383.
[23] R. Murr, J.I. Loizou, Y.G. Yang, C. Cuenin, H. Li, Z.Q. Wang, Z. Herceg, Histone acetylation by Trrap-Tip60 modulated loading of repair proteins and repair of DNA double-strand breaks, Nat. Cell Biol. 8 (2006) 91–99.
[24] J.A. Aten, J. Stap, P.M. Krawczyk, C.H. van Oven, R.A. Hoebe, J. Essers, R. Kanaar, Dynamics of DNA double-strand breaks revealed by clustering of damaged chromosome domains, Science 303 (2004) 92–95.
[25] B.E. Nelms, R.S. Maser, J.F. MacKay, M.G. Lagally, J.H. Petrini, In situ visualization of DNA double-strand break repair in human fibroblasts, Science 280 (1998) 590–592.
[26] C. Lukas, F. Melander, M. Stucki, J. Falck, S. Bekker-Jensen, M. Goldberg, Y. Lerenthal, S.P. Jackson, J. Bartek, J. Lukas, Mdc1 couples DNA double-strand break recognition by Nbs1 with its H2AX-dependent chromatin retention, EMBO J. 23 (2004) 2674–2683.
[27] M. Kozubek, S. Kozubek, E. Lukasova, A. Mareckova, E. Bartova, M. Skalnikova, A. Jergova, High-resolution cytometry of FISH dots in interphase cell nuclei, Cytometry 36 (1999) 279–293.
[28] M. Kozubek, S. Kozubek, E. Lukasova, E. Bartova, M. Skalnikova, P. Matula, P. Matula, P. Jirsova, A. Cafourkova, I. Koutna, Combined confocal and wide-field high-resolution cytometry of fluorescent in situ hybridization-stained cells, Cytometry 45 (2001) 1–12.
[29] M. Kozubek, P. Matula, P. Matula, S. Kozubek, Automated acquisition and processing of multidimensional image data in confocal in vivo microscopy, Microsc. Res. Tech. 64 (2004) 164–175.
[30] T. Kouzaridez, Histone acetylases and deacetylases in cell proliferation, Curr. Opin. Genet. Dev. 9 (1999) 40–48.
[31] A.J. Bannister, P. Zergman, J.F. Partridge, E.A. Miska, J.O. Thomas, R.C. Allshire, T. Kouzarides, Selective recognition of methylated lysine 9 on histone H3 by the HP1 chromo domain, Nature 410 (2001) 120–124.
[32] W.H. Lachner, D. O'Carroll, S. Rea, K. Mechtler, T. Jenuwein, Methylation of histone H3 Lysine 9 creates a binding site for HP1 proteins, Nature 410 (2001) 116–120.
[33] S. Khorasanizadeh, The nucleosome: from genomic organization to genomic regulation, Cell 116 (2004) 259–272.
[34] J.H. Petrini, T.H. Stracker, The cellular response to DNA double-strand breaks: defining the sensors and mediators, Trends Cell Biol. 13 (2003) 458–462.
[35] R.K. Sachs, A.M. Chen, D.J. Brenner, Proximity effects in the production of chromosome aberrations by ionizing radiation, Int. J. Radiat. Biol. 71 (1997) 1–19.
[36] I.B. Nazarov, A.N. Smirnova, R.I. Krutilina, M.P. Svetlova, L.V. Solovjeva, A.A. Nikiforov, S.L. Oei, I.A. Zalenskaya, P.M. Yau, E.M. Bradbury, N.V. Tomilin, Dephosphorylation of histone gamma-H2AX during repair of DNA double-strand breaks in mammalian cells and its inhibition by calyculin A, Radiat. Res. 160 (2003) 309–317.
[37] K. Rothkamm, M. Löbrich, Evidence for a lack of DNA double-strand break repair in human cells exposed to very low X-ray doses, Proc. Natl. Acad. Sci. U. S. A. 100 (2003) 5057–5062.
[38] N.N. Bhat, B.S. Rao, Dose rate effect on micronuclei induction in cytokinesis blocked human peripheral blood lymphocytes, Radiat. Prot. Dosim. 106 (2003) 45–52.
[39] Vijayalaxmi, K.S. Bisht, W.F. Pickard, M.L. Meltz, J.L. Roti Roti, E.G. Moros, Chromosome damage and micronucleus formation in human blood lymphocytes exposed in vitro to radiofrequency radiation at a cellular telephone frequency (847.74 MHz, CDMA), Radiat. Res. 156 (2001) 430–432.
[40] R.T. Abraham, Cell cycle checkpoint signalling through the ATM and ATR kinases, Genes Dev. 15 (2001) 2177–2196.